Effects of Lifshitz Transitions in Ferromagnetic Superconductors: The Case of URhGe

Yury Sherkunov, Andrey V. Chubukov, and Joseph J. Betouras

Phys. Rev. Lett. **121**, 097001 — Published 31 August 2018

DOI: 10.1103/PhysRevLett.121.097001

Effects of Lifshitz transitions in ferromagnetic superconductors: the case of URhGe

Yury Sherkunov[1], Andrey V. Chubukov[2] and Joseph J. Betouras[1]
[1]*Department of Physics and Centre for the Science of Materials, Loughborough University, Loughborough, LE11 3TU, United Kingdom and*
[2]*Department of Physics, University of Minnesota, Minneapolis, Minnesota 55455, USA*
(Dated: August 6, 2018)

In ferromagnetic superconductors, like URhGe, superconductivity co-exists with magnetism near zero field, but then re-appears again in a finite field range, where the system also displays mass enhancement in the normal state. We present the theoretical understanding of this non-monotonic behavior. We explore the multi-band nature of URhGe and associate re-entrant superconductivity and mass enhancement with the topological transition (Lifshitz) in one of the bands in a finite magnetic field. We found excellent agreement between our theory and a number of experimental results for URhGe, such as weakly first order reentrant transition, the dependence of superconducting T_c on a magnetic field, and the field dependence of the effective mass, the specific heat and the resistivity in the normal state. Our theory can be applied to other ferromagnetic multi-band superconductors.

Ferromagnetic superconductors are exciting systems to study the interplay of magnetism and superconductivity, contrary to the common wisdom that the presence of a ferromagnetic order destroys superconductivity. The coexistence of superconductivity and ferromagnetism has been realised experimentally for uranium-based heavy-fermion compounds, like UGe_2 [1], UCoGe [2] and URhGe [3]. The materials exhibit a wealth of exotic properties, including, e.g., the appearance of non-Landau damping in magnetic excitations [4].

Among these systems, URhGe has attracted much attention both experimentally [5–17] and theoretically [18–20]. In zero applied magnetic field, it displays ferromagnetism with magnetic moment oriented along the c -axis, and spin-triplet superconductivity at a lower temperature [6]. In an external magnetic field along the b-axis ($\mathbf{b} \perp \mathbf{c}$), superconductivity disappears at about B=2T. This is believed to be caused by the orbital effect of the field [6]. However, at higher magnetic fields, in the range from 8T to 13.5T, it reappears again [5] (see Fig.1).

Ferromagnetic spin fluctuations are believed to provide the pairing glue for superconductivity in a ferromagnetic metal [19, 20]. Indeed, NMR spin-spin relaxation measurements indicate that uniform longitudinal spin fluctuations (the ones in the direction of a magnetic field) are strongly enhanced in the field range where superconductivity has been observed [14]. Measurements of the specific heat [9, 10], electric conductivity [7, 9, 14, 15], and magnetisation [9] indicate that the increase of spin fluctuations is accompanied by the increase of the effective mass of fermions. This is indicative of a critical behavior near a ferromagnetic instability.

In this communication we address the origin of the ferromagnetic instability in a finite field. We argue that it is due to a Lifshitz transition observed [8] in one of the bands which form the electronic structure of URhGe. This Lifshitz transition pushes the system closer to the magnetic instability and enhances the magnetic fluctuations. This in turn leads to re-entrance of superconductivity (RSC) at a finite field.

The minimal model of the electronic structure of URhGe has two bands with non-equal dispersions (different masses m_1 and m_2) and band minima shifted by $\mathbf{K}_0$. (see Fig. 1). In a ferromagnetic state at zero field spin-up and spin-down states in both bands are split by an effective exchange field. Both branches of band 1 cross the chemical potential μ, while both branches of band 2 are above the chemical potential μ (see the left inset in Fig. 1). At a finite H the bands experience additional Zeeman splitting. The exchange field was reported [5] to be rather weak ($\sim 0.1T$), hence at fields near 10T Zeeman splitting dominates. The dispersions of the two bands with Zeeman splitting are $\epsilon_{1,\sigma}(\mathbf{k}) = \frac{\mathbf{k}^2}{2m_1} - \mu - \sigma\mu_B H$ and $\epsilon_{2,\sigma}(\mathbf{k}) = \frac{(\mathbf{k}-\mathbf{K}_0)^2}{2m_2} - \mu + \delta\mu - \sigma\mu_B H$, where $\delta\mu$ is the energy shift between bands 1 and 2 and σ is the projected value of the spin. As the field increases, the splitting grows, and at some critical field the system experiences a Lifshitz transition, in which spin-up branch of band 2 crosses the chemical potential (the middle inset in Fig. 1). We add the Hubbard four-fermion repulsive interaction U, the same for inter-band and intra-band scattering, and analyze the tendency towards magnetic order and magnetically-mediate superconductivity in this field range. As we show [21], the contribution of the inter-band scattering to the susceptibility is weak given the large momentum separation of the two bands. The fitting parameters relevant to URhGe are presented in [22].

We first compute the longitudinal and transverse susceptibilities at $T = 0$. Within RPA we have [23]:

$$\chi_{\parallel}(q) = \sum_{\sigma} \frac{\chi_0^{\sigma}(q)}{1 - U^2\chi_0^{\sigma}(q)\chi_0^{-\sigma}(q)}, \tag{1}$$

$$\chi_{\perp}(q) = \sum_{\sigma} \frac{\chi_0^{\sigma,-\sigma}(q)}{1 - U\chi_0^{\sigma,-\sigma}(q)}. \tag{2}$$

where $\chi_0^{\sigma} = \sum_{i=1,2} \chi_0^{i,i,\sigma,\sigma}$ and $\chi_0^{\sigma,-\sigma} = \sum_{i=1,2} \chi_0^{i,i,\sigma,-\sigma}$ are particle-hole susceptibilities of free fermions from the

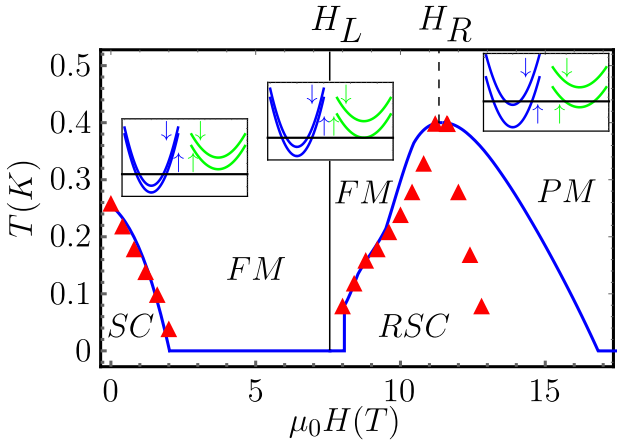

FIG. 1. The experimental and theoretical diagrams of URhGe in an external magnetic field H. Triangles are the experimental data [5], solid line is the theoretical result. Superconductivity is present near $H = 0$, absent at intermediate fields, and re-appears at higher fields, with a maximum at around $10 - 11$T. In the insets, we show the fermionic dispersion in our model of two electron bands, separated by $\mathbf{K}_0$ in the momentum space and exhibiting Zeeman splitting. The Lifshitz transition occurs at H_L, when the spin-up branch of band 2 touches the chemical potential. At higher H, this band opens up a new Fermi surface The maximum of T_c is at a field $H_R \sim 1.5 H_L$.

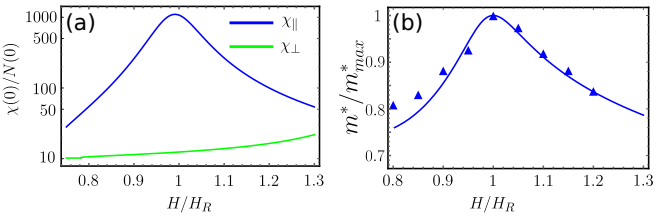

FIG. 2. (a) Longitudinal (blue/dark grey) and transverse (green/light grey) spin susceptibilities as functions of external magnetic field H/H_R. (b) The theoretical results for the effective mass of fermions in sub-band $1\downarrow$, $m^*_{1\downarrow}(H)$ (normalized to its maximum value at $H \approx H_R$) (solid line) along with m^* extracted from the measurements of magnetisation (triangles).[9].

two bands:

$$\chi_0^{j,i,\sigma,\sigma'}(\mathbf{q}, i\omega) = \int_l G_{j,\sigma}(\mathbf{l}, i\xi) G_{i,\sigma'}(\mathbf{l}+\mathbf{q}, i(\omega+\xi)), \quad (3)$$

where $G_{j,\sigma}(\mathbf{p}, i\omega) = (i\omega - \epsilon_{j\sigma}(\mathbf{p}))^{-1}$ and $\int_l ... = \int d\xi \frac{d^3 l}{(2\pi)^4} ....$ As the susceptibility $\chi(q)$ is enhanced at $q = 0$, the largest contribution to it comes from intra-band scattering because the two bands are shifted by a large momentum K_0.

The results are shown in Fig. 2 a. We see that the uniform longitudinal susceptibility is enhanced in the vicinity of the field H_R, which is somewhat larger than H_L, at which the Lifshitz transition occurs ($H_R \sim 1.5 H_L$). The non-monotonic behavior of $\chi_\parallel(q = 0)$ can be understood by noticing that the denominator in (1) behaves as

$$D = 1 - U^2 (N_{2\uparrow}(0) + N_{1\uparrow}(0)) N_{1\downarrow}(0), \quad (4)$$

where $N_{i\sigma}(0)$ is the density of states at the Fermi surface of a sub-band $i = 1, 2$ with spin projection σ. At $H > H_L$, $N_{2\uparrow}(0)$ becomes non-zero, D decreases and $\chi_\parallel(q = 0)$ increases. At higher fields $N_{1\downarrow}(0)$ decreases (see right insert in Fig. 1) and $\chi_\parallel(q = 0)$ decreases. At even higher magnetic field the spin-down sub-band of band 1 undergoes the second Lifshitz transition and becomes unoccupied, in agreement with [8]. The transverse $\chi_\perp(0)$ has much weaker dependence on $N_{2\uparrow}(0)$ and does not show a peak around H_R. This agrees with the NMR results [14].

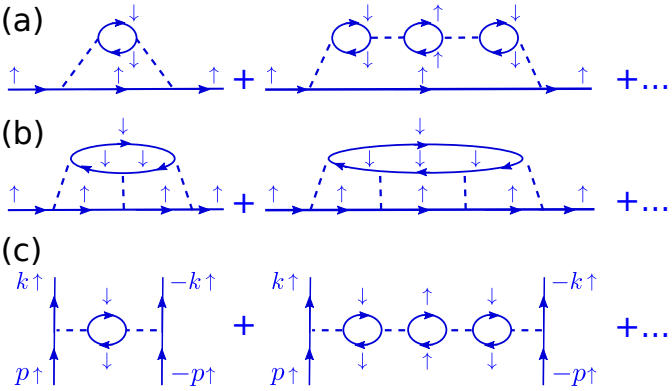

FIG. 3. Feynman diagrams describing the first two orders of the RPA series for (a) longitudinal component of the self-energy, $\Sigma^L_{i\uparrow}$; (b) transverse component of the self-energy, $\Sigma^T_{i\uparrow}$; and (c) p-wave pairing vertex.

The effective mass of a conduction electron is given by

$$\frac{m^*_{i\sigma}}{m_{i\sigma}} = [1 - \partial_\omega \Sigma_{i\sigma}(\mathbf{p}_{i\sigma F}, \omega)]_{\omega=0}, \quad (5)$$

The electron self-energy Σ can be written as a sum of longitudinal and transverse components. The corresponding ring and ladder diagrams [23, 24] are shown in Fig. 3 a and b, respectively:

$$\Sigma^L_{i\sigma}(\mathbf{p}, i\omega) = \int_q G_{i\sigma}(\mathbf{p}-\mathbf{q}, i(\omega-\xi)) V_L^{-\sigma}(\mathbf{q}, i\xi), \quad (6)$$

$$\Sigma^T_{i\sigma}(\mathbf{p}, i\omega) = \int_q G_{i,-\sigma}(\mathbf{p}-\mathbf{q}, i(\omega-\xi)) V_T^{\sigma,-\sigma}(\mathbf{q}, i\xi), \quad (7)$$

where the effective interactions are

$$V_L^{-\sigma}(\mathbf{q}, i\omega) = \frac{U^2 \chi_0^{-\sigma}(\mathbf{q}, i\omega)}{1 - U^2 \chi_0^{-\sigma}(\mathbf{q}, i\omega) \chi_0^{\sigma}(\mathbf{q}, i\omega)}, \quad (8)$$

$$V_T^{\sigma,-\sigma}(\mathbf{q}, i\omega) = \frac{U^3 [\chi_0^{\sigma,-\sigma}(\mathbf{q}, i\omega)]^2}{1 - U \chi_0^{\sigma,-\sigma}(\mathbf{q}, i\omega)}, \quad (9)$$

Again neglecting the weak inter-band scattering (i.e., the scattering between band 1 and band 2 [21]) in the calculation of susceptibilities, but retaining the dependence of

self-energies on all diagonal susceptibilities, we perform the frequency integration and, following [23, 24], we obtain

$$\frac{m^*_{i\sigma}}{m_{i\sigma}} = 1 + \lambda^{i\sigma}_L + \lambda^{i\sigma}_T, \tag{10}$$

where

$$\lambda^{i\sigma}_L = \frac{m_i}{(2\pi)^2 p_{Fi\sigma}} \int_0^{2p_{Fi\sigma}} q dq V_L^{-\sigma}(\mathbf{q}, 0), \tag{11}$$

$$\lambda^{i\sigma}_T = \frac{m_i}{(2\pi)^2 p_{Fi\sigma}} \int_{p_l}^{p_u} q dq V_T^{\sigma,-\sigma}(\mathbf{q}, 0). \tag{12}$$

Here $p_{Fi\sigma}$ is the Fermi momentum of the sub-band $\{i, \sigma\}$, and the integration limits for the transverse component are $p_l = max\{p_{Fi\sigma} - p_{Fi,-\sigma}, 0\}$ and $p_u = p_{Fi\sigma} + p_{Fi,-\sigma}$.

The result of the calculation of $m^*_{i\sigma}/m_{i\sigma}$ for the sub-band $1\downarrow$ is shown in Fig. 2 b. As expected, the mass enhancement is peaked at $H \approx H_R$, where the uniform susceptibility is the largest. The effective masses for other sub-bands show similar enhancement [21]. The theoretical result m^*/m agrees well with the mass ratio extracted from magnetisation measurements [9] (see Fig. 2 b). Using the result for $m^*(H)$, we computed the specific heat and resistivity. The main contribution to the specific heat comes from the $1\downarrow$ sub-band, and the Sommerfeld coefficient $\gamma = C(T)/T$ can be estimated as [25] $\gamma \propto N_{1\downarrow}(0) m^*_{1\downarrow}/m_1$. In Fig. 4a we show the calculated γ and the experimental one from Ref. [9]. Clearly, both are peaked around H_R and show similar behavior at smaller and higher fields. In Fig. 4 b we show theoretical and experimental results for the prefactor A in the expression for the resistivity $\rho = AT^2$. Theoretical A has been obtained using the Kadowaki - Woods relation [26] $A/\gamma^2 = const$, the experimental results are from Ref. [15]. Again, the agreement is quite good.

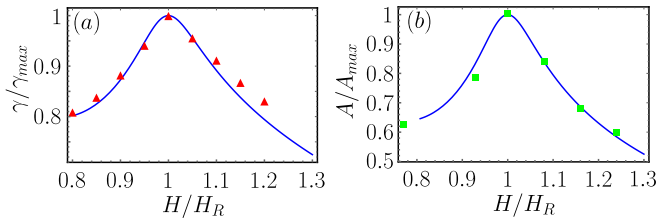

FIG. 4. Enhancement of (a) Sommerfeld coefficient γ measured in [9] (triangles) and (b) conductivity coefficient A measured in Ref [15] (squares) and calculated with our model (solid line) for the same parameters as in Fig. 1.

We next turn to superconductivity. The reduction and subsequent disappearance of superconductivity at small fields has been argued to be due to the orbital effect in a field [6, 27]. The reduction of T_c due to a vector potential close to T_c follows [27]

$$T_c(H) = T_c(H=0)\left(1 - H/H_c\right), \quad H_c = \frac{20\pi k_B^2 T_c^2(0)}{7\zeta(3) e\hbar v_F^2 \mu_0} \tag{13}$$

where k_B is the Boltzmann constant, μ_0 is the vacuum permeability. This form of $T_c(H)$ agrees with the data at small fields [6]. When $H > H_c$, $T_c(H)$ vanishes.

To study the re-entrant superconductivity, we do the analysis in two steps. First, we compute T_c^{Eli} within Eliashberg spin-fluctuation formalism, without including the orbital effect of a field. We then use the result for T_c^{Eli} as an effective $T_c(0)$ to estimate H_c from (13). We then use the full non-linear dependence of H_c on T_c (13) to obtain the actual T_c for the polar p-wave state.

An exchange by ferromagnetic spin fluctuations enhances the pairing vertex in p-wave channel, and below we search for superconducting order with p-wave symmetry. We analyze all fields and keep both Zeeman and exchange splitting. To keep calculations under control, we neglect the feedback from ferromagnetic order on the pairing interaction. This feedback is relevant near a ferromagnetic quantum-critical point [28], but less relevant away from criticality, where our analysis holds.

In Eliashberg theory one needs to solve the set of equations for quasiparticle $Z_{i\sigma}(\mathbf{q}, i\omega_n) = 1 - \Sigma_{i\sigma}(\mathbf{q}, i\omega_n)/(i\omega_n)$ and the pairing vertex, $W_{i\sigma}$:

$$(1 - Z_{i\sigma}(p)) i\omega_n = T \sum_{p'} \frac{V_z^{-\sigma}(p - p') Z_{i\sigma}(p') i\omega_{n'}}{(i\omega_{n'} Z_{i\sigma}(p'))^2 - \epsilon_{i\sigma}(\mathbf{p}')^2}, \tag{14}$$

$$W_{i\sigma}(p) = T \sum_{p'} \frac{V_W^{-\sigma}(p - p') W_{i\sigma}(p')}{(i\omega_{n'} Z_{i\sigma}(p'))^2 - \epsilon_{i\sigma}(\mathbf{p}')^2}, \tag{15}$$

where $\sum_{p'} ... = \sum_{\omega_{n'}} \int d^3p' ...$, $\omega_n = \pi(2n+1)T$, $p = \{\mathbf{p}, i\omega_n\}$, and the interactions are $V_z^{-\sigma} = V_L^{-\sigma} + V_T^{\sigma,-\sigma}$ and $V_W^{-\sigma} = V_L^{-\sigma}$. We use a standard trick and reduce Eliashberg set to a single equation by introducing $\Phi(p) = W(p)/|\omega_n Z(p)|$. Then $\Phi(p)$ is expanded in spherical harmonics and only the p-wave piece, $\Phi^1_{i\sigma}$ is retained. Integrating over momenta as $\int d^3p ... = \int d\Omega \int d\epsilon N_{i\sigma}(0) ...$, where Ω is the solid angle, we obtain an integral equation of $\Phi^1_{i\sigma}(\omega_n)$ in the form

$$\sum_{n \geq 0} K_{mn}(\omega_m \omega_n) \Phi^1_{i\sigma}(\omega_n) = 0, \tag{16}$$

where

$$K_{mn} = \lambda^{(1)}_{-\sigma}(\omega_m - \omega_n) + \lambda^{(1)}_{-\sigma}(\omega_m + \omega_n) - \delta_{mn} \left| \sum_{l=-N-1}^{N} \lambda^{(0)}_{-\sigma}(\omega_m - \omega_l) sgn(\omega_l) + \frac{\omega_m}{\pi T} \right|, \tag{17}$$

We introduced $\lambda^{(1)}_{-\sigma} = -N_{i\sigma}(0) \int d\Omega Y_1(\cos(\theta)) V_W^{-\sigma}(\theta)$ and $\lambda^{(0)}_{-\sigma} = N_{i\sigma}(0) \int d\Omega V_z^{-\sigma}(\theta)$, where $Y_1(\theta)$ is the first spherical harmonic and θ is the angle between $\mathbf{p}$ and $\mathbf{p}'$.

Keeping only the interaction with small momentum transfer, we factorize the pairing between three bands: up and down sub-bands of band 1 and spin-up sub-band

of band 2. We recall, however, that effective p-wave pairing interaction between fermions on a given band is the sum of contributions from particle-hole bubbles from all three bands. We solve Eq. (17) for all three bands and find the largest T_c (see [21] for details). The result is shown as a solid line in Fig. 5a. At smaller fields $H < H^*$, where H^* is slightly above H_L, superconductivity develops on the $1\uparrow$ sub-band. At at $H > H^*$ it switches to sub-band $1\downarrow$, and T_c for superconductivity on this band has a maximum at $H \sim H_R$, where the effective mass on this band is also maximal. We next include the orbital effect. In Fig. 5b we show H_c from Eq. 13 as a function of external H. Orbital effect destroys superconductivity when $H_c < H$. We see that this holds at intermediate fields, in the range where without orbital effect superconductivity would develop at sub-band $1\uparrow$. At higher fields, superconductivity switches to sub-band $1\downarrow$, where the effective mass and $T_c^{Eli}(H)$ are larger, and k_F is smaller. It is worth noticing that the orbital effects gets reduced when the upper critical field $H_c \propto (m*/k_F)^2$ gets larger. In our model, k_F is reduced while m^* increases near the field, where the system undergoes the Lifshitz transition. Therefore the orbital effect is less effective at larger fields. We show the actual T_c by dashed line in Fig. 5 b and by solid line in Fig. 1. Note that T_c appears discontinuously at $H = H^*$, where T^{Eli} switches from $1\uparrow$ to $1\downarrow$ sub-band. Inter-band pairing interactions likely smoothen the first-order phase transition. The theoretical profile of T_c vs H agrees nicely with the data [5] (see Fig. 1).

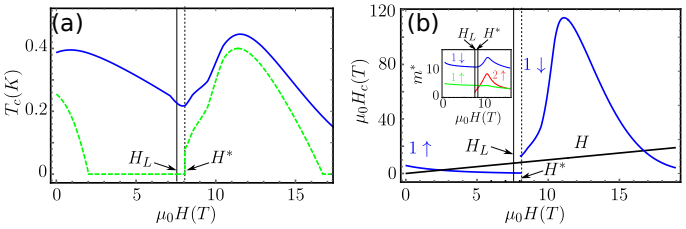

FIG. 5. (a) Solid line – $T_c^{Eli}(H)$, obtained within Eliashberg formalism without including the orbital effect of the field. Dashed line – the actual T_c, with both Zeeman/exchange and orbital effects. The actual T_c is always smaller than $T_c^{Eli}(H)$ due to the orbital effect of the external and the exchange fields. (b) The effective field H_c from Eq. 13 as a function of H. The orbital effect destroys superconductivity when H_c (blue line) is smaller than H (thin black line). The value of H_c changes discontinuously at $H = H^*$, when superconductivity switches from sub-band $1\uparrow$ to sub-band $1\downarrow$, where the effective mass is larger. This gives rise to a jump in the actual T_c in panel (a). The effective mass over the whole range is presented in the inset.

To summarize, in this communication we argued that the enhancement of the effective mass in URhGe at fields near 10 T and the emergence of RSC around this field are due to Lifshitz transition. We considered the model for URhGe with two electronic bands and analyzed the behavior of the system near a field when the bottom of the spin-up branch of previously unoccupied band 2 sinks below the Fermi level. We first computed the transverse and longitudinal spin susceptibilities and argued that the longitudinal susceptibility dramatically enhances in some field range above the Lifshitz transition, while the transverse susceptibility remains flat. This fully agrees with the behavior of longitudinal and transverse susceptibilities, extracted from NMR measurements of the relaxation times, $1/T_1$ and $1/T_2$ [14]. We next computed the one-loop self-energy due to magnetically-mediated interaction and obtained the enhancement of the effective mass. The theoretical result for m^*/m agrees with the experimental data extracted from magnetisation measurements [9, 29]. There were also very good agreements for the Sommerfeld coefficient and the prefactor for the T^2 term in the resistivity [9, 15].

Then, we turned to the analysis of the superconductivity. We first solved the Eliashberg equation for magnetically-mediated superconductivity without the orbital effect of the applied field and obtained T_c^{Eli} with a maximum at a field where the effective mass is the largest. Superconductivity resides on $1\uparrow$ sub-band at smaller fields and on $1\downarrow$ sub-band at higher fields. We then took into account the pair-breaking orbital effect and found that superconductivity exists at small fields, gets destroyed by orbital effect at intermediate fields, and re-appears discontinuously roughly at a field of Lifshitz transition. This behavior fully agrees with the data [5] (Fig. 1). The reduction of theoretical T_c at higher fields is somewhat slower than in the data. One reason could be a re-orientational transition, detected at 12T [5], in which the magnetic moment rotates towards the field direction, leaving its magnitude unchanged. This spin re-orientation does not increase longitudinal fluctuations but complicates the field dependence of T_c above 12T. Overall, it looks increasingly likely that topological Fermi-surface transitions can account for much of the puzzling physics in nearly magnetic itinerant systems [30, 31].

We thank R. Fernandes and M. Greven for useful conversations. This work was supported by the EPSRC (YS and JJB) through the grant EP/P002811/1. and by the U.S. Department of Energy through the University of Minnesota Center for Quantum Materials, under award DE-SC-0016371 (A.V.C.).

[1] S. S. Saxena, P. Agarwal, F. M. Grosche, R. K. W. Haselwimmer, M. J. Steiner, E. Pugh, I. R. Walker, P. Julian, S. R.and Monthoux, G. G. Lonzarich, I. Huxley, A. Sheikin, et al., Nature **406**, 587 (2000).

[2] N. T. Huy, A. Gasparini, D. E. de Nijs, Y. Huang, J. C. P. Klaasse, T. Gortenmulder, A. de Visser, A. Hamann, T. Gorlach, and H. Lohneysen, Phys. Rev. Lett. **99**,

067006 (2007).
[3] D. Aoki, A. Huxley, E. Ressouche, D. Braithwaite, J. Flouquet, J.-P. Brison, E. Lhotel, and C. Paulsen, Nature **413**, 613 (2001).
[4] A. V. Chubukov, J. J. Betouras, and D. V. Efremov, Phys. Rev. Lett. **112**, 037202 (2014).
[5] F. Lévy, I. Sheikin, B. Grenier, and A. D. Huxley, Science **309**, 1343 (2005).
[6] F. Hardy and A. D. Huxley, Phys. Rev. Lett. **94**, 247006 (2005).
[7] A. Miyake, D. Aoki, and J. Flouquet, Journal of the Physical Society of Japan **77**, 094709 (2008).
[8] E. A. Yelland, J. M. Barraclough, W. Wang, K. V. Kamenev, and A. D. Huxley, Nature Physics **7**, 890 (2011).
[9] F. Hardy, D. Aoki, C. Meingast, P. Schweiss, P. Burger, H. v. Löhneysen, and J. Flouquet, Phys. Rev. B **83**, 195107 (2011).
[10] D. Aoki, T. D. Matsuda, F. Hardy, C. Meingast, V. Taufour, E. Hassinger, I. Sheikin, C. Paulsen, G. Knebel, H. Kotegawa, et al., Journal of the Physical Society of Japan **80**, SA008 (2011).
[11] D. Aoki, G. Knebel, and J. Flouquet, Journal of the Physical Society of Japan **83**, 094719 (2014).
[12] D. Aoki and J. Flouquet, Journal of the Physical Society of Japan **83**, 061011 (2014).
[13] S.-i. Fujimori, I. Kawasaki, A. Yasui, Y. Takeda, T. Okane, Y. Saitoh, A. Fujimori, H. Yamagami, Y. Haga, E. Yamamoto, et al., Phys. Rev. B **89**, 104518 (2014).
[14] Y. Tokunaga, D. Aoki, H. Mayaffre, S. Krämer, M.-H. Julien, C. Berthier, M. Horvatić, H. Sakai, S. Kambe, and S. Araki, Phys. Rev. Lett. **114**, 216401 (2015).
[15] A. Gourgout, A. Pourret, G. Knebel, D. Aoki, G. Seyfarth, and J. Flouquet, Phys. Rev. Lett. **117**, 046401 (2016).
[16] F. Wilhelm, J. P. Sanchez, J.-P. Brison, D. Aoki, A. B. Shick, and A. Rogalev, Phys. Rev. B **95**, 235147 (2017).
[17] D. Braithwaite, D. Aoki, J.-P. Brison, J. Flouquet, G. Knebel, A. Nakamura, and A. Pourret, Phys. Rev. Lett. **120**, 037001 (2018).
[18] K. Hattori and H. Tsunetsugu, Phys. Rev. B **87**, 064501 (2013).
[19] V. P. Mineev, Phys. Rev. B **91**, 014506 (2015).
[20] V. P. Mineev, Phys. Usp. **60**, 121 (2017).
[21] See Supplementary Materials, which include Ref. [32–35].
[22] The parameters of the electronic structure are $m_1 = 8.06 \times 10^{-28} kg$, $m_2 = 2.4m_1$, $v_{F0} = 10434 m/s$, $\delta\mu/\epsilon_F^0$ =1.48. For the calculation of superconductivity we used $UN(0) = 1.03$. Here $\epsilon_F^0 = [3n(2\pi)^2/4]^{2/3}/(2m_1)$, $v_{F0} = \sqrt{\frac{2\epsilon_F^0}{m_1}}$, and $N(0) = \frac{m_1^{3/2}(\epsilon_F^0)^{1/2}}{2^{1/2}\pi^2}$ are the Fermi energy, Fermi velocity and density of states in the absence of exchange and external magnetic fields. n is the total electron density.
[23] W. F. Brinkman and S. Engelsberg, Phys. Rev. **169**, 417 (1968).
[24] D. Fay and J. Appel, Phys. Rev. B **22**, 3173 (1980).
[25] A. C. Jacko, J. O. Fjaerestad, and B. J. Powell, Nature Physics **5**, 422 (2009).
[26] K. Kadowaki and S. B. Woods, Solid State Communications **58**, 507 (1986).
[27] K. Scharnberg and R. A. Klemm, Phys. Rev. B **22**, 5233 (1980).
[28] A. V. Chubukov, A. M. Finkel'stein, R. Haslinger, and D. K. Morr, Phys. Rev. Lett. **90**, 077002 (2003).
[29] Our model explains the quantitative disagreement between the effective masses extracted from magnetization, specific heat and transport measurements [9]. This is because of the extraction method: the effective mass in [9] was calculated under the assumption that the Fermi momentum does not change with the external magnetic field. However, in our model, the Fermi momentum is a function of magnetic field due to the Lifshitz transition.
[30] S. Slizovskiy, A. V. Chubukov, and J. J. Betouras, Phys. Rev. Lett. **114**, 066403 (2015).
[31] S. Slizovskiy, J. J. Betouras, S. T. Carr, and J. Quintanilla, Phys. Rev. B **90**, 165110 (2014).
[32] P. B. Allen and R. C. Dynes, Phys. Rev. B **12**, 905 (1975).
[33] K. Levin and O. T. Valls, Phys. Rev. B **17**, 191 (1978).
[34] T. R. Kirkpatrick and D. Belitz, Phys. Rev. B **67**, 024515 (2003).
[35] M. Kagan and A. Chubukov, JETP Lett **50**, 517 (1989).